Grand Valley State University

ScholarWorks@GVSU

Peer Reviewed Articles   Chemistry Department

6-21-2016

A three-dimensional He−CO potential energy surface with improved long-range behavior

George C. McBane
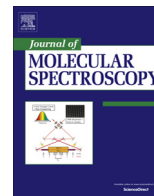
Grand Valley State University, mcbaneg@gvsu.edu

Follow this and additional works at: https://scholarworks.gvsu.edu/chm_articles

Part of the Chemistry Commons

A three-dimensional He–CO potential energy surface with improved long-range behavior

George C. McBane

Department of Chemistry, Grand Valley State University, Allendale, MI 49401 USA

ABSTRACT

A weakness of the "CBS + corr" He–CO potential energy surface (Peterson and McBane, 2005) has been rectified by constraining the potential to adopt accurate long-range behavior for He–CO distances well beyond $15a_0$. The resulting surface is very similar to the original in the main part of the interaction. Comparison with accurately known bound-state energies indicates that the surface is slightly improved in the region sampled by the highest lying bound states. The positions of shape and Feshbach resonances within a few cm^{-1} of the $j = 1$ excitation threshold are essentially unchanged. The low-energy scattering lengths changed noticeably. The revised surface generates a small negative limiting scattering length for collisions with ^{4}He, while the original surface gave a small positive one. Both surfaces yield scattering lengths quite different from the widely used surface of Heijmen et al. (1997) for both He isotopes.

© 2016 The Author. Published by Elsevier Inc. This is an open access article under the CC BY-NC-ND license (http://creativecommons.org/licenses/by-nc-nd/4.0/).

1. Introduction

Carbon monoxide, the most common polar diatomic molecule in space, is widely used as a gauge of local conditions in astrophysics [1]. Interpretation of astronomical CO spectral observations requires knowledge of its interactions with the most common colliders H, H_2, and He. An influential 1976 article by Green and Thaddeus [2] introduced many in the chemical dynamics community to the astrophysical importance of CO collisions. The He–CO system has served as a benchmark for the study of weak intermolecular interactions since then.

More than a dozen He–CO potential energy surfaces have been described since 1976. Peterson and McBane gave a brief review and comparison of many of them [3]. The most influential and widely used of these surfaces include the *ab initio* surfaces of Diercksen and coworkers [4,5], the empirical XC(fit) surface of Le Roy and coworkers [6], and the "symmetry adapted perturbation theory" *ab initio* surface of Heijmen et al. [7].

CO is relatively convenient to study experimentally, and a wide variety of measurements have been made. Leading references appear in papers by Thachuk et al. [8], Reid et al. [9], McKellar and coworkers [10], McCourt et al. [11], Carty et al. [12], and Amaral et al. [13]. Two notable recent papers report measurements of very low-energy scattering resonances [14] and polarization-dependent state-to-state inelastic differential cross sections [15].

Two high-quality He + CO potential energy surfaces in current use are the symmetry-adapted perturbation theory (SAPT) potential of Heijmen et al. [7] and the "CBS + corr" potential of Peterson and McBane [3]. The SAPT potential was constructed with a perturbation technique based on accurate monomer electronic wavefunctions for CO and He. The CBS + corr potential was constructed with a sequence of "supermolecule" calculations on the HeCO complex at the CCSD(T) level, followed by extrapolation to an approximate complete basis set limit and a small correlation-energy correction. Both potentials treat the dependence on the CO bond length with low-order polynomial expansions. The SAPT potential uses an analytic model function fitted to the *ab initio* points. The CBS + corr potential uses the "reproducing kernel Hilbert space" (RKHS) interpolation technique [16] in the Jacobi coordinates R and γ, followed by least-squares polynomial expansion in the CO bond length. While the two surfaces are quite similar, the SAPT potential has a smaller repulsive core, a deeper (by about $1.4\ cm^{-1}$) well, and a larger (by $0.36\ cm^{-1}$) dissociation energy from the ground state than CBS + corr. The spacings between levels on the SAPT potential are slightly larger than those on CBS + corr. This difference is reflected in predictions of spectroscopic transitions on the two surfaces. Line positions predicted with SAPT tend to fall at higher frequencies than experimental ones, while those predicted with CBS + corr tend to fall at lower frequencies than experiment [3].

The RKHS interpolation technique yields a surface that extrapolates to large R with behavior of the form $-\sum_n C_n/R^n$, with the number of terms in the expansion selectable by the choice of

E-mail address: mcbaneg@gvsu.edu

kernel function. Peterson and McBane used a kernel whose long-range behavior included C_6 and C_7 terms. The long-range coefficients were not constrained, but adopted whatever values provided the smoothest match to the *ab initio* points being interpolated. Ho and Rabitz have pointed out that such free extrapolation, while it gives the correct qualitative form of the long-range potential, does not usually give accurate C_n coefficients [17]. Peterson and McBane therefore cautioned in their paper that while the absolute errors in their extrapolated function were small, large relative errors could be expected in the potential at distances well beyond the $15a_0$ distance of their outermost *ab initio* points and the potential could not be recommended for computation of properties that depended on the very long range behavior.

Ho and Rabitz have described a method [17] for constraining the values of the long-range coefficients in RKHS surfaces. With their method it is possible to modify the extrapolation behavior of the CBS + corr potential to give better accuracy at long range, while using the same accurate *ab initio* data to determine the main part of the potential. This paper describes the construction and properties of such an improved CBS + corr potential.

2. Potential modifications

The *ab initio* data used for the original CBS + corr potential were computed on a rectangular grid of Jacobi coordinates, using seven values of the CO bond length r_{CO}, 18 values of the distance R from the CO center of mass to He, and ten angles γ between those two vectors; $\gamma = 0$ corresponds to the He–O–C linear arrangement. To evaluate the potential $V(r_{CO}, R, \gamma)$, two-dimensional RKHS evaluations were carried out to determine $V(r_{CO}, R, \gamma)$ for each of the seven r_{CO} in the *ab initio* grid, and then a cubic polynomial fit of those seven energies was used to generate the potential at the desired r_{CO}. The RKHS evaluations had the form

$$V(R, \gamma) = \sum_i \alpha_i Q(R_i, \gamma_i, R, \gamma) \tag{1}$$

where the index i runs over all the (R, γ) pairs in the *ab initio* grid, α_i is a set of coefficients determined at the start of the program, and $Q(R, \gamma, R', \gamma')$ is the kernel function. Q is given by

$$Q(R, \gamma, R', \gamma') = q_1^{2,5}(R, R')q_2^2(\gamma, \gamma'), \tag{2}$$

where the distance kernel $q_1^{n,m}(R, R')$ and the angle kernel $q_2^{n_2}(\gamma, \gamma')$ are defined in Eqs. (17) and (23) of Ho and Rabitz [16]. (In practice the angle kernel is not defined directly on γ but instead on a scaled angle variable $x = (1 - \cos \gamma)/2$.) The superscript indices on the distance kernel $q_1^{n,m}(R, R')$ determine the long-range behavior [17,18]: the number of inverse-power terms present in the expansion is n, and the lowest inverse power involved is $m + 1$. All the work described here uses $m = 5$ to give a leading asymptotic behavior $V(R) \sim -C_6/R^6$.

The coefficients α_i are determined by solving the set of linear equations that uses the known energy at each *ab initio* point as the "target",

$$\sum_i Q(R_i, \gamma_i, R_j, \gamma_j)\alpha_i = V(R_j, \gamma_j), \tag{3}$$

or, in more compact form,

$$\sum_i \Gamma_{ij}\alpha_i = \beta_j, \tag{4}$$

where $\Gamma_{ij} = Q(R_i, \gamma_i, R_j, \gamma_j)$ and $\beta_j = V(R_j, \gamma_j)$. There are $n_R n_\gamma = 180$ (R, γ) pairs in the *ab initio* grid so this is a set of 180 linear equations, one for each value of j. One such set must be solved at each of the seven values of r_{CO} in the grid, yielding seven sets of 180 coefficients.

To constrain the long-range behavior of the RKHS evaluation using a set of known C_{nL} long-range coefficients, additional "virtual" points are added to the *ab initio* grid [17]. These new points have R values at user-selected distances in the long-range region, and use the same γ values as the original grid. The number of new R values added must equal n_{LR}, the number of long-range coefficients C_n to be constrained, so the total number of new equations in the set is $n_{LR}n_\gamma$. The expanded set of linear equations can still be written in the form (4), with new definitions of Γ_{ij} and β_j when $j > n_R n_\gamma$:

$$\Gamma_{ij} = \frac{A_{nmk}R_i^k}{R_a^{m+k+1}} \tag{5}$$

$$\beta_j = \frac{-C_{m+k+1}(\gamma_j)}{R_a^{m+k+1}}. \tag{6}$$

Here $k = 0, 1, \ldots, n_{LR} - 1$ indexes the added values of R. A_{nmk}, a component of the distance kernel $q_1^{n,m}(R, R')$, is a combinatorial coefficient defined in Eq. (7) of Ref. [17]. R_a is a user-selected "constraint distance", optimally chosen at a distance where the asymptotic terms C_n/R^n have comparable values. $C_n(\gamma_j)$ is an angle-specific long-range coefficient,

$$C_n(\gamma) = \sum_{L=0}^{n-4} C_{nL}P_L(\cos \gamma) \tag{7}$$

where P_L is a Legendre polynomial and the C_{nL} are restricted to even values of $n + L$.

Hettema et al. published [19] a computed set of C_{nL} coefficients for He–CO in 1993, and it appears to remain the most recent explicitly described set. However, the group that produced the SAPT potential, which includes some of the same authors, computed a more extensive set with better quality that is included in tabular form in the code for evaluating the potential [7]. This more extensive set includes n values up to 12 and L values up to 6, and includes the dependence on r_{CO} as a polynomial expansion. These coefficients have been selected to constrain the long-range behavior of the revised CBS + corr potential at distances well beyond the outermost *ab inito* points at $R = 15a_0$.

The choice of n in the RKHS distance kernel $q_1^{n,m}(R, R')$ influences not only the asymptotic behavior but also the smoothness and numerical stability of the RKHS interpolation procedure. The interpolated function has n continuous derivatives, and therefore becomes both smoother and "stiffer" as n increases. In addition, the condition number of Eq. (4) tends to increase with increasing n, and regularization techniques may become necessary. The original Peterson and McBane potentials were all constructed with a $q_1^{2,5}(R, R')$ distance kernel, giving C_6 and C_7 terms in the region beyond $R = 15a_0$. Numerical tests showed that in the region of most interest here, $15a_0 \leqslant R \leqslant 30a_0$, the C_7 and C_8 terms were of similar magnitude while C_9 and higher terms were much smaller. For the present revised potential the $q_1^{3,5}(R, R')$ distance kernel was therefore chosen, giving $V(R) \sim -C_6/R^6 - C_7/R^7 - C_8/R^8$ behavior asymptotically. A constraint distance $R_a = 10a_0$ was used.

The remaining task in setting up a long-range-constrained version of the CBS + corr potential is to select the n_{LR} new distances R to be used. Beyond the outermost new distance, the potential will have exactly the constrained behavior. Inside the last *ab initio* grid point with smaller R than the innermost new distance, the potential will be determined primarily by the *ab initio* data, though the effect of the constraints will penetrate to some extent because of the smoothness properties of the interpolation. The region in between is a matching region, and the goal is to get as smooth and physically reasonable a junction behavior as possible.

Ho and Rabitz suggested that all the new distances be chosen beyond the range of the *ab initio* points, and adopted that approach in both their initial examples [17]. However, in the present study, every selection of three distances beyond $15a_0$ tested resulted in relatively poor joining behavior. Smooth and reasonable behavior was found when the innermost virtual point was placed at $12.5a_0$, halfway between the last two values of R on the original grid. Once that choice was made, the resulting potential was not very sensitive to the placement of the two remaining virtual points at larger R; $20a_0$ and $30a_0$ were finally selected. The Γ matrix of Eq. (4) was not as well conditioned as for the original unconstrained $q_1^{2.5}(R,R')$ version, but still of full rank, and the system could be solved in double precision without regularization.

Fig. 1 shows cuts of the original CBS + corr potential, the new potential, and a trial version of the new potential made with long-range distances of 20, 25, and $30a_0$. The task of joining the long-range and interior parts of the potential smoothly is most difficult at the carbon end of the molecule, so the curves are shown at $\gamma = 160°$. The top panel shows $V(R)$ itself in the long-range region for the three different RKHS curves, and indicates that the differences among all these potentials are small in absolute terms. The lower panel shows $R^6 V(R)$, which approaches the constant value $-C_6(\gamma)$ asymptotically. This presentation is designed to magnify differences and problems at long range. The blue curve ("$C_6 + C_7 + C_8$") in the lower panel shows, in the same presentation, the long-range dispersion/induction curve that the new potential is constrained to follow beyond $R = 30a_0$. The original, unconstrained CBS + corr potential shows smooth behavior but goes eventually toward an inaccurate asymptotic C_6. The trial version of the constrained potential, whose smallest constraining R value is $20a_0$, does smoothly join the blue asymptotic curve around
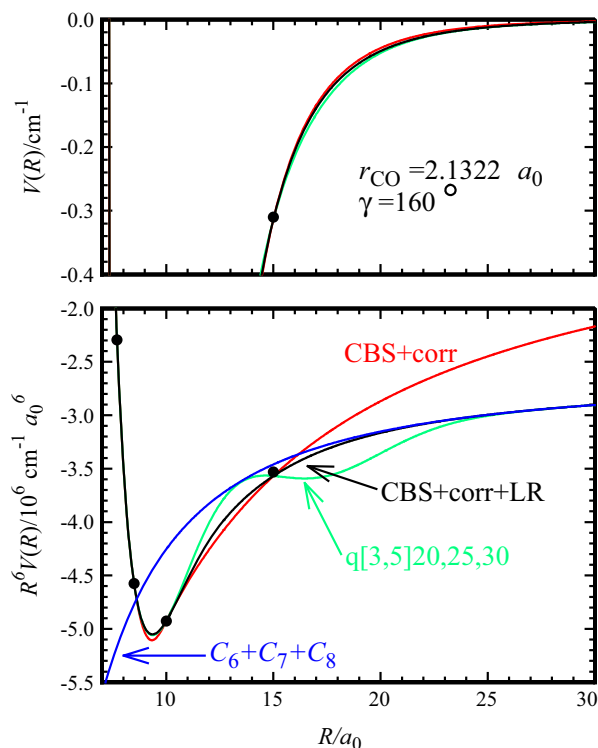
$R = 25a_0$, but its behavior in the region $10a_0 \leqslant R \leqslant 25a_0$ displays polynomial wiggles that indicate poor matching. The final version of the constrained potential, whose smallest constraining R value is $12.5a_0$, is much smoother. It differs modestly from the original CBS + corr potential for $R < 15a_0$, but merges with the desired asymptotic curve shortly thereafter.

Careful inspection of Fig. 1 shows that the three RKHS curves all agree with one another at the final normal-grid distance $15a_0$ but do not pass exactly through the plotted *ab initio* point. This discrepancy does not represent interpolation error. The seven two-dimensional RKHS interpolations yield surfaces that do pass through the *ab initio* points for each value of r_{CO}. The evaluated 3D potential, however, is not constructed by interpolation through those seven points, but instead by evaluating the best-fit cubic polynomial through them. That polynomial is not likely to pass exactly through any one of the points used in its construction.

Fortran code to evaluate the original CBS + corr potential is available as electronic supplementary material associated with Ref. [3]. Additional files that extend that support to the revised CBS + corr + LR potentials are available as supplementary material with this article.

3. Bound states of HeCO

The nuclear wavefunctions of the HeCO van der Waals complex are principally contained in the main part of the potential well. The computed energies of those states would therefore not be expected to change much when modifications to the long-range tail of the potential are introduced. Small changes might appear either because the constraints produce changes to the surface within the main well, or because the wavefunctions extend into the long-range region. The relative energies of all but one of the states have been accurately determined by spectroscopic experiments [10,20–23].

Tables 1 and 2 show energies of the HeCO bound states computed with the original CBS + corr, the modified CBS + corr + LR, and the SAPT potentials for ^{3}He and ^{4}He. The levels are labeled in the approximate-free-rotor scheme with the total angular momentum quantum number J and the approximate quantum numbers j for CO rotation and l for end-over-end rotation of the complex. These energies were computed with the BOUND program of Hutson [24], using the physical values and numerical parameters described in section III B of Ref. [3]. The calculations used 2D versions of the potentials constructed by averaging over the vibrational wavefunctions of CO; this approximation was found to be excellent by both Heijmen et al. and Peterson and McBane.

Most energies presented here for the SAPT potential lie within 0.001 cm^{-1} of those presented by Heijmen et al. [7]. The (0, 1, 1) level is a notable exception. The present calculations for ^{4}HeCO find it 0.0036 cm^{-1} closer to the ground state than reported in the SAPT paper. For ^{3}HeCO it is 0.0122 cm^{-1} closer to the ground state.

Changes in the energies of the bound states introduced by the long-range constraints are small, as expected. The absolute energies of the ground states increase by roughly 0.0035 cm^{-1} for both isotopomers. For ^{3}He–CO in $v = 0$, only two level energies change by more than 0.001 cm^{-1} with respect to the ground state. They belong to the two most weakly bound levels: the (0, 1, 1), whose binding energy is 0.075 cm^{-1}, and the (2, 1, 1), bound by 0.434 cm^{-1}. Both changes modestly improve the agreement with experiment compared to the original CBS + corr potential. The (0, 1, 1) level, in particular, has the most extended wavefunction of all the bound levels, as measured by its average $\langle R \rangle$ computed within BOUND by the perturbation method of Hutson [25]. It would be therefore be expected to be the most sensitive to changes

Fig. 1. Potential curves from the original CBS + corr potential, a trial version of the new constrained potential ("q[3,5] 20,25,30"), the final constrained potential ("CBS + corr + LR"), and (in the lower panel only) the constraining asymptotic curve ("$C_6 + C_7 + C_8$"), all for $r_{CO} = 2.1322a_0$ and $\gamma = 160°$. The upper panel shows $V(R)$ itself; the lower panel, $R^6 V(R)$. Energies from the *ab initio* grid are shown as black dots.

Table 1

Energy levels (in cm^{-1}) of the ^{3}He–CO complex. The first row gives the absolute energy of the ground state with respect to separated He and CO. Subsequent rows give the energy of each higher level with respect to $(0, 0, 0)$, and the unweighted root-mean-square error with respect to experiment for the entire set of levels. The experimental energies are those presented by Surin et al. [22]. The experimental value in brackets is an estimate [21].

(J, j, l)	$v = 0$				$v = 1$			
	CBS + corr	CBS + corr + LR	SAPT	Expt	CBS + corr	CBS + corr + LR	SAPT	Expt
$(0, 0, 0)$	−5.2236	−5.2199	−5.5417		−5.2466	−5.2426	−5.5859	
$(0, 1, 1)$	5.1426	5.1458	5.2009	5.1775	5.1332	5.1379	5.1691	5.1629
$(1, 0, 1)$	0.6966	0.6967	0.7068	0.7003	0.6960	0.6961	0.7065	0.6997
$(1, 1, 0)$	3.9625	3.9631	3.9913	3.9748	3.9296	3.9303	3.9639	3.9423
$(1, 1, 1)$	4.3679	4.3672	4.4225	4.3843	4.3351	4.3344	4.3990	4.3518
$(2, 0, 2)$	2.0648	2.0651	2.0966	2.0738	2.0631	2.0635	2.0959	2.0721
$(2, 1, 1)$	4.7843	4.7862	4.8138	4.8004	4.7513	4.7534	4.7840	4.7673
$(2, 1, 2)$	5.7853	5.7849	5.8608	5.8069	5.7520	5.7516	5.8370	5.7735
$(3, 0, 3)$	4.0417	4.0424	4.1103	4.0608	4.0394	4.0402	4.1101	4.0582
$(3, 1, 3)$	7.8261	7.8261	7.9363	[7.856]	7.7926	7.7928	7.9130	7.8233
rms error	0.0203	0.0196	0.0803		0.0195	0.0185	0.0452	

Table 2

Energy levels (in cm^{-1}) of the ^{4}He–CO complex, as in Table 1. The experimental values are those presented by Potapov et al. [23].

(J, j, l)	$v = 0$				$v = 1$			
	CBS + corr	CBS + corr + LR	SAPT	Expt	CBS + corr	CBS + corr + LR	SAPT	Expt
$(0, 0, 0)$	−6.4308	−6.4276	−6.7880		−6.4553	−6.4519	−6.8360	
$(0, 1, 1)$	5.3782	5.3859	5.3518	5.3904	5.3475	5.3559	5.3079	5.3593
$(1, 0, 1)$	0.5741	0.5742	0.5817	0.5763	0.5735	0.5736	0.5812	0.5762
$(1, 1, 0)$	3.9796	3.9799	4.0174	3.9954	3.9467	3.9470	3.9920	3.9636
$(1, 1, 1)$	4.2496	4.2490	4.3079	4.2677	4.2172	4.2165	4.2858	4.2360
$(1, 1, 2)$	6.0725	6.0790	6.1013	6.0953	6.0484	6.0556	6.0654	6.0699
$(2, 0, 2)$	1.7102	1.7103	1.7332	1.7171	1.7083	1.7086	1.7320	1.7157
$(2, 1, 1)$	4.7165	4.7180	4.7492	4.7342	4.6828	4.6843	4.7205	4.7012
$(2, 1, 2)$	5.4239	5.4234	5.4974	5.4467	5.3906	5.3902	5.4748	5.4147
$(3, 0, 3)$	3.3804	3.3808	3.4281	3.3944	3.3771	3.3776	3.4261	3.3915
$(3, 1, 2)$	5.9112	5.9137	5.9535	5.9336	5.8772	5.8798	5.9232	5.8999
$(3, 1, 3)$	7.1463	7.1461	7.2440	7.1759	7.1121	7.1120	7.2208	7.1431
$(4, 0, 4)$	5.5300	5.5309	5.6155	5.5556	5.5257	5.5267	5.6137	5.5507
$(4, 1, 4)$	9.3537	9.3539	9.4875	9.3934	9.3191	9.3195	9.4645	9.3603
rms error	0.0214	0.0203	0.0441		0.0219	0.0208	0.0503	

in the long-range potential. For ^{4}He–CO, the two levels bound by less than 1 cm^{-1}, $(1, 1, 2)$ and $(3, 1, 2)$, again improve by 0.0025 cm^{-1} or more. The $(0, 1, 1)$ level, bound by 1.04 cm^{-1}, also improves substantially, but the $(2, 1, 2)$ level, bound by 1.00 cm^{-1}, is essentially unchanged. No other level energies change by more than 0.0015 cm^{-1}. The behavior for $v = 1$ is very similar to that for $v = 0$. The unweighted root-mean-square error for the entire set of bound state energies improves by about 5% for both isotopomers. This rms error is roughly 0.02 cm^{-1} for the CBS + corr + LR potential, and 0.04–0.05 cm^{-1} for the SAPT potential.

Each isotopomer supports two "parity-bound" levels, which cannot dissociate to $j = 0$ CO. While their absolute energies are high, they are more strongly bound than some lower-lying levels that can dissociate to $j = 0$. Their energies are little affected by the potential modification.

4. Scattering resonances

Bergeat et al. recently measured inelastic cross sections for rotational excitation of CO in very low energy collisions [14]. The collision energy range includes the excitation threshold for the $0 \rightarrow 1$ transition. At collision energies not more than about 10 cm^{-1} above the threshold, substantial resonance structure is predicted by scattering calculations. The finite energy resolution of the experiment somewhat obscured the resonance structure but the main features were clearly discernable.

Near-threshold cross sections were computed by Cecchi-Pestellini et al. [26] in 2002 using the SAPT surface. Bergeat et al. computed the expected resonance structures for both the SAPT and CBS + corr surfaces, and resolved them into contributions from specific shape and Feshbach resonances. The predictions from the two surfaces are very similar, but the resonance energies predicted by SAPT are consistently a few tenths of cm^{-1} below those from CBS + corr. This difference reflects the lower absolute energies (that is, greater binding energies) of most bound levels on the SAPT surface. No clear discrimination between the two surfaces could be made by comparison to experiment, though the onset of the first resonance above threshold did appear to match the SAPT prediction better.

Fig. 2 shows the $0 \rightarrow 1$ inelastic cross sections computed from the original CBS + corr, new CBS + corr + LR, and SAPT surfaces. They were computed using the MOLSCAT program of Hutson and Green [27] with the hybrid log-derivative Airy propagator of Manolopoulos and Alexander [28,29]. The channel basis included CO rotational states up to $j = 10$ and the propagations were carried out to a distance of at least 30 Å.

The original and revised CBS + corr results are nearly identical; the position of the initial resonance shifts by about 0.01 cm^{-1} to higher energy on the revised surface. The small effect of the long-range modifications on these resonance positions is not surprising. Like the bound state wavefunctions, the wavefunctions associated with shape and Feshbach resonances are principally located within the main part of the potential well. Most of the PES region that affects the resonance positions is therefore determined by the *ab initio* energies and is little affected by the changes at very long range. Even though the resonances are "low-energy features", the original CBS + corr potential was well characterized in the relevant potential regions.
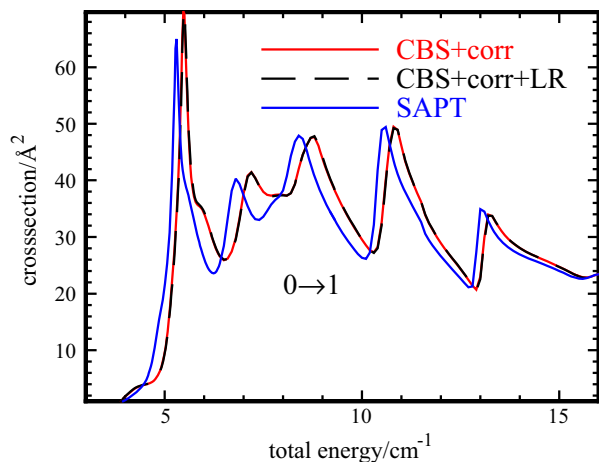
Fig. 2. Cross sections for the CO $0 \rightarrow 1$ rotational transition.

5. Low energy scattering lengths

The s-wave scattering length [30,31] should be sensitive to changes in the long-range part of the He–CO potential. For total energies below the $j = 1$ threshold, only single-channel scattering is possible and the scattering length a must be real. It goes to a constant value in the limit of low collision energy, and is an important parameter in the characterization of low-temperature collisions [32]. In the low-energy limit the elastic cross section is $\sigma = 4\pi a^2$. Limiting scattering lengths for the SAPT potential have been computed for several CO initial states and for both ^{3}He and ^{4}He by Balakrishnan et al. [33], Zhu et al. [34], and Bodo and Gianturco [35].

Scattering lengths for He–CO collisions were computed with a recent version of MOLSCAT [36], using the 2D $v = 0$ averaged versions of the potentials and limiting the total angular momentum to $J = 0$. The propagations were carried out to a distance of 200 Å to ensure the potential energy was negligible compared to the kinetic energy down to the lowest energies. Scattering lengths were computed from the S-matrix elements using the expression of Hutson [31].

Fig. 3 shows scattering lengths and $0 \rightarrow 0$ partial cross sections for ^{4}He–CO collisions as a function of collision energy for the original CBS + corr, new CBS + corr + LR, and SAPT potentials. The scattering lengths do indeed change noticeably among the three potentials. The CBS + corr potential gives a limiting scattering length that is positive but near zero (+0.19 Å) at low energy. The modifications, which strengthen the long-range attractions slightly, move the limiting scattering length to a negative value, −0.25 Å. (This change is a smooth one; simply multiplying the CBS + corr + LR potential by a vertical scaling factor λ that varies from 0.98 to 1.02 smoothly shifts the limiting scattering length from +0.93 Å to −1.58 Å.) The elastic scattering cross sections for both versions of the CBS + corr potential are correspondingly small. The scattering length on the revised potential goes through a zero crossing near $E = 4.5 \times 10^{-3}$ cm^{-1}, and its elastic cross section shows a corresponding $\sigma = 0$ minimum at the same energy.

The SAPT potential shows a more typical behavior. Its limiting scattering length is also negative but much larger in magnitude, −3.56 Å, and at low energy its elastic cross section is roughly 160 Å^2. The SAPT scattering length shows a zero crossing at
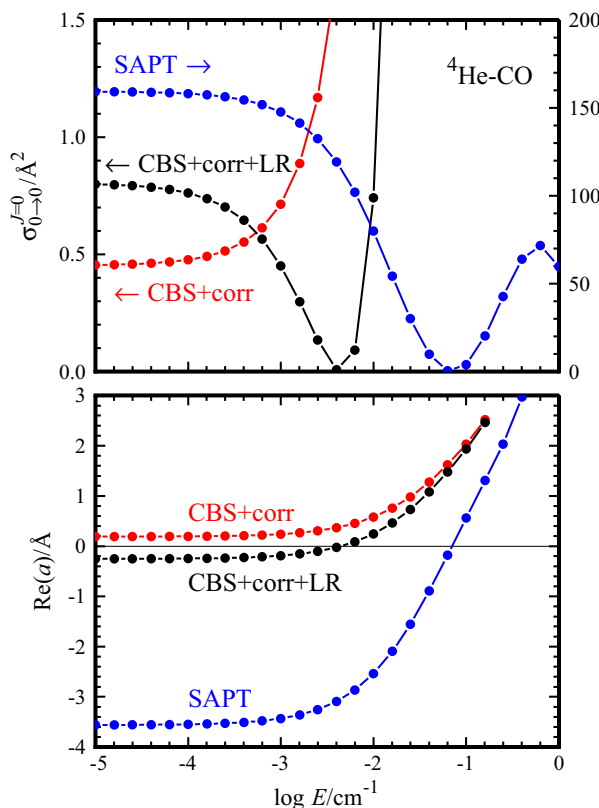

Fig. 3. s-wave scattering lengths (lower panel) and $J = 0$ partial elastic cross sections (upper panel) for the $j = 0$ channel of ^{4}He–CO collisions in the low energy regime. Note the different vertical scales for the Peterson and McBane and SAPT potentials in the upper panel.
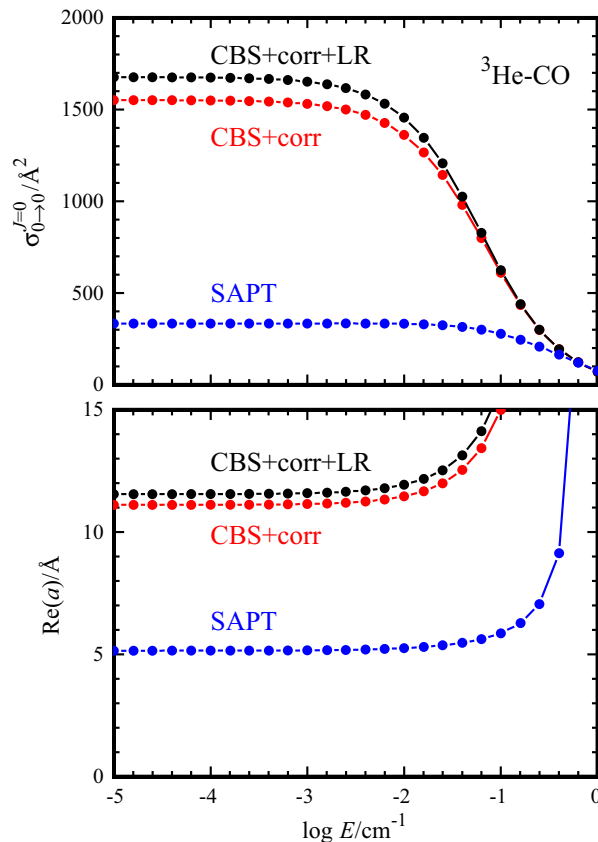

Fig. 4. s-wave scattering lengths (lower panel) and $J = 0$ partial elastic cross sections (upper panel) for the $j = 0$ channel of ^{3}He–CO collisions in the low energy regime.

$E = 0.07$ cm^{-1}. The values obtained here are in excellent agreement with those reported by others [33–35].

The behavior for ^{3}He–CO, shown in Fig. 4, is different. All three potentials show positive limiting scattering lengths at low energy. Their elastic cross sections increase with decreasing energy before reaching large constant values. The limiting cross sections from both CBS + corr potentials are larger by roughly a factor of five than those from the SAPT potential.

The scattering length is affected by both the long-range potential and the inner region [37]. The quantitatively different behavior of the SAPT and CBS + corr + LR potentials shows that while the very long range part of the latter has been constrained to essentially match that of the SAPT potential, its overall physical properties even at very low temperature do not simply reproduce those of the SAPT potential.

6. Conclusion

The new CBS + corr + LR surface is very slightly changed from the original [3] in the main part of the potential well. Comparison with accurately known bound-state energies indicates that the surface is slightly improved in the region sampled by the highest lying bound states. The positions of shape and Feshbach resonances within a few cm^{-1} of the $j = 1$ excitation threshold are essentially unchanged. The low-energy scattering lengths, however, did change noticeably. The revised surface generates a small negative limiting scattering length for collisions with ^{4}He, while the original surface gave a small positive one. Both surfaces yield scattering lengths and limiting elastic cross sections quite different from the widely used SAPT surface [7] for both He isotopes.

Acknowledgements

Appendix A. Supplementary material

Supplementary data associated with this article can be found, in the online version, at http://dx.doi.org/10.1016/j.jms.2016.06.004.

References

[1] A.D. Bolatto, M. Wolfire, A.K. Leroy, The CO-to-H$_2$ conversion factor, Ann. Rev. Astron. Astrophys. 51 (1) (2013) 207–268.
[2] S. Green, P. Thaddeus, Rotational excitation of CO by collisions with He, H, and H$_2$ under conditions in interstellar clouds, Astrophys. J. 205 (1976) 766–785.
[3] K.A. Peterson, G.C. McBane, A hierarchical family of three dimensional potential energy surfaces for He–CO, J. Chem. Phys. 123 (8) (2005) 084314 (Erratum in J. Chem. Phys., 124(22) (2006) 229901).
[4] L.D. Thomas, W.P. Kraemer, G.H.F. Diercksen, Rotational excitation of CO by He impact, Chem. Phys. 51 (1980) 131–139.
[5] R. Schinke, G.H.F. Diercksen, Vibrational relaxation of CO($n = 1$) in collisions with He, J. Chem. Phys. 83 (9) (1985) 4516–4521.
[6] R.J. Le Roy, C. Bissonnette, T.H. Wu, A.K. Dham, W.J. Meath, Improved modelling of atom-molecule potential-energy surfaces: illustrative application to He–CO, Farad. Disc. 97 (1994) 81–94.
[7] T.G.A. Heijmen, R. Moszynski, P.E.S. Wormer, A. van der Avoird, New He-CO interaction energy surface with vibrational coordinate dependence. 1. *Ab initio* potential and infrared spectrum, J. Chem. Phys. 107 (1997) 9921–9928.
[8] M. Thachuk, C.E. Chuaqui, R.J. Le Roy, Linewidths and shifts of very low temperature CO in He: a challenge for theory or experiment?, J Chem. Phys. 105 (1996) 4005–4014.
[9] J. Reid, C. Simpson, H. Quiney, A new He–CO interaction energy surface with vibrational coordinate dependence. 2. The vibrational deactivation of CO ($v = 1$) by inelastic collisions with ^{3}He and ^{4}He, J. Chem. Phys. 107 (1997) 9929–9934.
[10] A.R.W. McKellar, Y. Xu, W. Jager, C. Bissonnette, Isotopic probing of very weak intermolecular forces: microwave and infrared spectra of CO–He isotopomers, J. Chem. Phys. 110 (1999) 10766–10773.
[11] F. McCourt, M. ter Horst, E. Heck, A. Dickinson, Transport properties of He–CO mixtures, Mol. Phys. 100 (24) (2002) 3893–3906.
[12] D. Carty, A. Goddard, I.R. Sims, I.W.M. Smith, Rotational energy transfer in collisions between CO ($X^1\Sigma^+$, $v = 2, J = 0, 1, 4$, and 6) and He at temperatures from 294 to 15 K, J. Chem. Phys. 121 (10) (2004) 4671–4683.
[13] G.A. Amaral, F.J. Aoiz, L. Banares, J. Barr, V.J. Herrero, B. Martinez-Haya, M. Menendez, G.A. Pino, I. Tanarro, I. Torres, J.E. Verdasco, Low-temperature rotational relaxation of CO in self-collisions and in collisions with Ne and He, J. Phys. Chem. A 109 (42) (2005) 9402–9413.
[14] A. Bergeat, J. Onvlee, C. Naulin, A. van der Avoird, M. Costes, Quantum dynamical resonances in low-energy CO($j = 0$) + He inelastic collisions, Nat. Chem. 7 (2015) 349–353.
[15] L. Song, G.C. Groenenboom, A. van der Avoird, C.K. Bishwakarma, G. Sarma, D. H. Parker, A.G. Suits, Inelastic scattering of CO with He: polarization dependent differential state-to-state cross sections, J. Phys. Chem. A 119 (2015) 12526–12537.
[16] T.-S. Ho, H. Rabitz, A general method for constructing multidimensional molecular potential energy surfaces from *ab initio* calculations, J. Chem. Phys. 104 (7) (1996) 2584–2597.
[17] T.-S. Ho, H. Rabitz, Proper construction of *ab initio* global potential surfaces with accurate long-range interactions, J. Chem. Phys. 113 (10) (2000) 3960–3968.
[18] P. Soldan, J.M. Hutson, On the long-range and short-range behavior of potentials from reproducing kernel Hilbert space interpolation, J. Chem. Phys. 112 (9) (2000) 4415–4416.
[19] H. Hettema, P.E.S. Wormer, A.J. Thakkar, Intramolecular bond-length dependence of the anisotropic dispersion coefficients for interactions of rare-gas atoms with N$_2$, CO, Cl$_2$, HCl and HBr, Mol. Phys. 80 (1993) 533–548.
[20] C.E. Chuaqui, R.J. Le Roy, A.R.W. McKellar, Infrared spectrum and potential energy surface of He–CO, J. Chem. Phys. 101 (1994) 39–61.
[21] M.-C. Chan, A.R.W. McKellar, Observation of strong hidden lines in the infrared spectrum of the CO–He complex, J. Chem. Phys. 105 (1996) 7910–7914.
[22] L.A. Surin, D.A. Roth, I. Pak, B.S. Dumesh, F. Lewen, G. Winnewisser, Detection of the millimeter wave spectra of the weakly bound complexes ^{3}He–CO and ^{4}He–CO, J. Chem. Phys. 112 (9) (2000) 4064–4068.
[23] A.V. Potapov, L.A. Surin, V.A. Panfilov, B.S. Dumesh, Millimeter-wave spectroscopy of weakly bound molecular complexes: Isotopologues of He–CO, Opt. Spectrosc. 106 (2) (2009) 183–189.
[24] J.M. Hutson, BOUND computer code, version 5, 1993, distributed by Collaborative Project No. 6 of the Science and Engineering Research Council (UK).
[25] J. Hutson, Coupled channel bound-state calculations – calculating expectation values without wavefunctions, Chem. Phys. Lett. 151 (6) (1988) 565–569.
[26] C. Cecchi-Pestellini, E. Bodo, N. Balakrishnan, A. Dalgarno, Rotational and vibrational excitation of CO molecules by collision with ^{4}He atoms, Astrophys. J. 571 (2002) 1015–1020.
[27] J.M. Hutson, S. Green, MOLSCAT computer code, version 14, 1994, distributed by Collaborative Computational Project No. 6 of the Engineering and Physical Sciences Research Council (UK), Available at <http://www.giss.nasa.gov/tools/molscat/>.
[28] D.E. Manolopoulos, An improved log derivative method for inelastic scattering, J. Chem. Phys. 85 (1986) 6425–6429.
[29] M.H. Alexander, D.E. Manolopoulos, A stable linear reference potential algorithm for solution of the quantum close-coupled equations in molecular scattering theory, J. Chem. Phys. 86 (1987) 2044–2050.
[30] N. Balakrishnan, V. Kharchenko, R. Forrey, A. Dalgarno, Complex scattering lengths in multi-channel atom-molecule collisions, Chem. Phys. Lett. 280 (1-2) (1997) 5–9.
[31] J.M. Hutson, Feshbach resonances in ultracold atomic and molecular collisions: threshold behaviour and suppression of poles in scattering lengths, New J. Phys. 9 (2007) 152.
[32] R.V. Krems, W.C. Stwalley, B. Friedrich (Eds.), Cold Molecules: Theory, Experiment, Applications, CRC Press, 2009.
[33] N. Balakrishnan, A. Dalgarno, R.C. Forrey, Vibrational relaxation of CO by collisions with ^{4}He at ultracold temperatures, J. Chem. Phys. 113 (2) (2000) 621–627.
[34] C. Zhu, N. Balakrishnan, A. Dalgarno, Vibrational relaxation of CO in ultracold ^{3}He collisions, J. Chem. Phys. 115 (3) (2001) 1335–1339.
[35] E. Bodo, F. Gianturco, Collisional cooling of polar diatomics in ^{3}He and ^{4}He buffer gas: a quantum calculation at ultralow energies, J. Phys. Chem. A 107 (37) (2003) 7328–7336.
[36] J.M. Hutson, MOLSCAT computer code, version 16, May 2012, distributed by Collaborative Computational Project No. 6 of the Engineering and Physical Sciences Research Council (UK).
[37] G.F. Gribakin, V.V. Flambaum, Calculation of the scattering length in atomic collisions using the semiclassical approximation, Phys. Rev. A 48 (1993) 546–553.